Early Prediction and Impact Assessment of CYP3A4-Related Drug-Drug Interactions for Small-Molecule Anticancer Drugs Using Human-CYP3A4-Transgenic Mouse Models[S]

David Damoiseaux, Jos H. Beijnen, Alwin D.R. Huitema, and Thomas P.C. Dorlo

Department of Pharmacy & Pharmacology, The Netherlands Cancer Institute, Amsterdam, The Netherlands (D.D., J.H.B., A.D.R.H., T.P.C.D.); Utrecht Institute of Pharmaceutical Sciences (J.H.B.) and Department of Clinical Pharmacy, University Medical Center Utrecht (A.D.R.H.), Utrecht University, Utrecht, The Netherlands; Department of Pharmacology, Princess Máxima Center for Pediatric Oncology, Utrecht, The Netherlands (A.D.R.H.); and Department of Pharmacy, Uppsala University, Uppsala, Sweden (T.P.C.D.)

ABSTRACT

Early detection of drug-drug interactions (DDIs) can facilitate timely drug development decisions, prevent unnecessary restrictions on patient enrollment, resulting in clinical study populations that are not representative of the indicated study population, and allow for appropriate dose adjustments to ensure safety in clinical trials. All of these factors contribute to a streamlined drug approval process and enhanced patient safety. Here we describe a new approach for early prediction of the magnitude of change in exposure for cytochrome P450 (P450) CYP3A4-related DDIs of small-molecule anticancer drugs based on the model-based extrapolation of human-CYP3A4-transgenic mice pharmacokinetics to humans. Victim drugs brigatinib and lorlatinib were evaluated with the new approach in combination with the perpetrator drugs itraconazole and rifampicin. Predictions of the magnitude of change in exposure deviated at most 0.99- to 1.31-fold from clinical trial results for inhibition with itraconazole, whereas exposure predictions for the induction with rifampicin were less accurate, with deviations of 0.22- to 0.48-fold. Results for the early prediction of DDIs and their clinical impact appear promising for CYP3A4 inhibition, but validation with more victim and perpetrator drugs is essential to evaluate the performance of the new method.

SIGNIFICANCE STATEMENT

The described method offers an alternative for the early detection and assessment of potential clinical impact of CYP3A4-related drug-drug interactions. The model was able to adequately describe the inhibition of CYP3A4 metabolism and the subsequent magnitude of change in exposure. However, it was unable to accurately predict the magnitude of change in exposure of victim drugs in combination with an inducer.

Introduction

Discovery and mapping of drug-drug interactions (DDIs) as early as practically possible to assure safety during clinical trials can pay off, as DDIs can have a profound negative impact on the benefit-risk balance of a drug. The investigation of DDIs of a novel compound with cytochrome P450 (P450) enzymes can be carried out in an in vitro setting, enabling early determination during drug development (https://www.fda.gov/media/134582/download). However, it is challenging to extrapolate these findings to in vivo conditions, especially in a quantitative manner, which is crucial for predicting the clinical impact of such interactions.

Clinical DDI studies are conducted before drug registration during phases II and III of clinical development. According to European Medicines Agency (EMA) and US Food and Drug Administration (FDA) guidelines, DDI studies have to be performed using strong inhibitors

and inducers to follow a worst-case approach (https://www.ema.europa.eu/en/documents/scientific-guideline/guideline-investigation-drug-interactions-revision-1_en.pdf; https://www.fda.gov/media/134581/download). Subsequently, physiologically based pharmacokinetic (PBPK) predictions are used to predict in silico the effects of moderate and weak inhibitors or inducers (perpetrator drugs) (https://www.fda.gov/media/101469/download). The performance of these clinical trials and subsequent PBPK model development and verification is time consuming. As a result, there is often a lack of clinical data on weak and moderate perpetrator drugs, which are more frequently used in the clinic than strong perpetrator drugs. PBPK simulations can help overcome this problem, but data may not always be available immediately after drug approval (Molenaar-Kuijsten et al., 2021).

Previous research described the development of an extrapolated population pharmacokinetic (PK) model for small-molecule anticancer drugs in human-CYP3A4-transgenic mice (a transgenic mouse model with its endogenous Cyp3a gene knocked out and replaced with the human CYP3A4 gene) that adequately predicted the human PK for brigatinib and lorlatinib (Damoiseaux et al., 2022). Predictability of the model for human PK can be validated, and misspecifications in interspecies extrapolation can be resolved using phase I trial results. Our

ABBREVIATIONS: AUC_{0-inf}, area under the plasma concentration-time curve from 0 until infinity; CL, clearance; DDI, drug-drug interaction; ER, extraction ratio; K_m, Michaelis-Menten constant; P450, cytochrome P450; PBPK, physiologically based pharmacokinetic; PK, pharmacokinetic; REA, relative enzyme activity; t_{max}, time of maximum plasma concentration.

hypothesis is that a human-CYP3A4-transgenic mouse can represent the situation of normal CYP3A4 enzyme activity and that a Cyp3a knockout mouse represents a situation in which CYP3A4 is fully inhibited. Subsequently, the inhibition or induction of CYP3A4 can be predicted as a fold difference between both mouse species. The fraction of CYP3A4 inhibition can be defined by the initial velocity equation appropriate for the mechanism of inhibition (competitive, uncompetitive, noncompetitive, or mixed). For induction, the rise in CYP3A4 activity from baseline by the perpetrator drug can be modeled using an enzyme turnover model (Yamashita et al., 2013). Our aim was to develop a method for early prediction of the magnitude of change in exposure for weak, moderate, and strong CYP3A4-related DDIs of small-molecule anticancer drugs as victim drugs using human-CYP3A4-transgenic mice.

Methods

Data. A selection of two victim drugs was made from previously developed human-CYP3A4-transgenic mouse models that were extrapolated to humans, lorlatinib and brigatinib, for which the human PK was adequately predicted and open-label crossover DDI studies were available (Damoiseaux et al., 2022). The model structures of the previously developed mouse models were a two-compartment model with dual first-order absorption for lorlatinib and a two-compartment model for brigatinib. These extrapolated mouse models represented normal human CYP3A4 activity without a DDI. The dataset that was used for the development of the mouse population PK models also contained PK data from Cyp3a knockout mice. The difference between Cyp3a knockout mouse PK and human-CYP3A4-transgenic mouse PK was described by covariates on clearance and bioavailability. The PK parameters derived from the Cyp3a knockout mouse were assumed to represent a fully inhibited CYP3A4 enzyme activity. Furthermore, population PK models from literature were used to simulate the PK of itraconazole, rifampicin, and the rifampicin induction dynamics of CYP3A4 (Hennig et al., 2007; Wilkins et al., 2008; Yamashita et al., 2013). Clinical trials in healthy participants investigating DDI of lorlatinib and brigatinib were used to evaluate the concordance of preclinical predictions and clinical observations of the fold change in exposure due to the DDI with the perpetrator drugs itraconazole and rifampicin (Chen et al., 2020; Patel et al., 2020; Tugnait et al., 2020).

Modeling of Inhibition. The DDIs of lorlatinib and brigatinib with itraconazole were modeled as a competitive inhibition, and the workflow for the predictions is summarized in Fig. 1 (model code can be found in Supplemental Model code DDI inhibition). The difference in clearance and bioavailability between the extrapolated Cyp3a knockout and human-CYP3A4-transgenic mouse was considered CYP3A4-related metabolism of the drug from 0% to 100%. This difference can be interpreted as the isolated CYP3A4-related effect on clearance and bioavailability. The isolated effect was then scaled according to the degree and rate of inhibition and reintegrated in the model.

To model the effect of CYP3A4 inhibition on clearance, the elimination rate constant for CYP3A4-related clearance ($k_{e,CYP3A4}$) was calculated as follows:

$$k_{e, CYP3A4} = k_{e, human-CYP3A4-transgenic} - k_{e, Cyp3a\, knock-out} \quad (1)$$

where $k_{e,human-CYP3A4-transgenic}$ represents the elimination rate constant of the extrapolated human-CYP3A4-transgenic mouse and $k_{e,Cyp3a\, knockout}$ represents the elimination rate constant of the extrapolated Cyp3a knockout mouse. The previously described extrapolations of both mouse models to human was performed by means of allometric scaling of clearance and volume of distribution with an exponent of 0.75 and 1, respectively (Damoiseaux et al., 2022).

The relative enzyme activity (REA) over time was calculated using the initial velocity equation for competitive inhibition:

$$REA = \frac{V_{max}[S]}{K_m\left(1 + \frac{[I]}{K_i}\right) + [S]} \quad (2)$$

where V_{max} is set to 1 to represent the relative maximal velocity of uninhibited CYP3A4-related clearance, K_m is the Michaelis-Menten constant of the substrate $[S]$ for CYP3A4, and K_i the dissociation constant of the inhibitor $[I]$. The K_i of itraconazole is 0.0157 μM (Isoherranen et al., 2004), and the K_m values of lorlatinib and brigatinib are 1.52 μM and not available, respectively (https://www.accessdata.fda.gov/drugsatfda_docs/nda/2018/210868Orig1s000MultidisciplineR.pdf). We evaluated K_m values of 0.1, 1, and 10 μM for brigatinib because brigatinib has a similar molecular structure as lorlatinib and therefore the K_m is probably in the same order of magnitude.

Subsequently, the elimination rate constant of lorlatinib and brigatinib in the presence of an inhibitor could be calculated as follows:

$$k_e = k_{e, Cyp3a\, knock-out} + k_{e, CYP3A4} \cdot REA \quad (3)$$

To describe the inhibitory effect on bioavailability, the reduction of bioavailability attributed to CYP3A4 metabolism was (F_{CYP3A4}) was determined first:

$$F_{CYP3A4} = F_{Cyp3a\, knock-out} - F_{human-CYP3A4-transgenic} \quad (4)$$

where $F_{Cyp3a\, knockout}$ is the bioavailability of the extrapolated Cyp3a knockout mouse and $F_{human-CYP3A4-transgenic}$ represents the bioavailability of the extrapolated human-CYP3A4-transgenic mouse.

The effect of CYP3A4 inhibition on bioavailability (F) was also described using the initial velocity equation for competitive inhibition (eq. 2):

$$F = F_{human-CYP3A4-transgenic} + F_{CYP3A4} \cdot (1 - REA) \quad (5)$$

Modeling of Induction. The effect of the inducer rifampicin on the PK of lorlatinib and brigatinib was modeled using a rifampicin-induced CYP3A4 turnover model (model code can be found in Supplemental Model code DDI induction) (Yamashita et al., 2013). The model was developed for the simulation of DDI once the blood concentration of the inducer reaches a steady state after repeated dosing. The prediction of the induction by this model, fold change induction ($CYP3A4_{fold\, induction}$), was subsequently used as REA for clearance.

As for the modeling of inhibition, the difference in clearance between the extrapolated Cyp3a knockout and human-CYP3A4-transgenic mouse was considered the isolated CYP3A4-related metabolism of the drug from 0% to 100%, for which the workflow is summarized in Fig. 1. To model the effect of CYP3A4 induction, the murine CYP3A4-related hepatic clearance ($CL_{H,CYP3A4,mouse}$) was calculated:

$$CL_{H, CYP3A4, mouse} = CL_{human-CYP3A4-transgenic} - CL_{Cyp3a\, knock-out} \quad (6)$$

with the $CL_{H,CYP3A4,mouse}$ and the hepatic blood flow in mice ($Q_{H,mouse}$) and humans ($Q_{H,human}$), the intrinsic clearance in humans ($CL_{int,human}$), the human CYP3A4 extraction ratio ($ER_{CYP3A4,human}$), and the human CYP3A4-related hepatic clearance ($CL_{H,CYP3A4,human}$) could be calculated following the well-stirred liver model equations (eq. 7–10). Hepatic blood flow in mice ($Q_{H,mouse}$) and humans ($Q_{H,human}$) are approximately 0.12 and 90 l/h, respectively (Lautt, 2009; Xie et al., 2014):

$$ER_{mouse} = \frac{CL_{H, CYP3A4, mouse}}{Q_{H, mouse}} \quad (7)$$

$$CL_{int, human} \cdot f_u = \frac{CL_{H, CYP3A4, mouse}}{1 - ER_{mouse}} \cdot \left(\frac{BWT_{human}}{BWT_{mouse}}\right)^{0.75} \quad (8)$$

$$ER_{CYP3A4, human} = \frac{CL_{int, human} \cdot f_u \cdot REA}{Q_{H, human} + CL_{int, human} \cdot f_u \cdot REA} \quad (9)$$

$$CL_{H, CYP3A4, human} = ER_{CYP3A4, human} \cdot Q_{H, human} \quad (10)$$
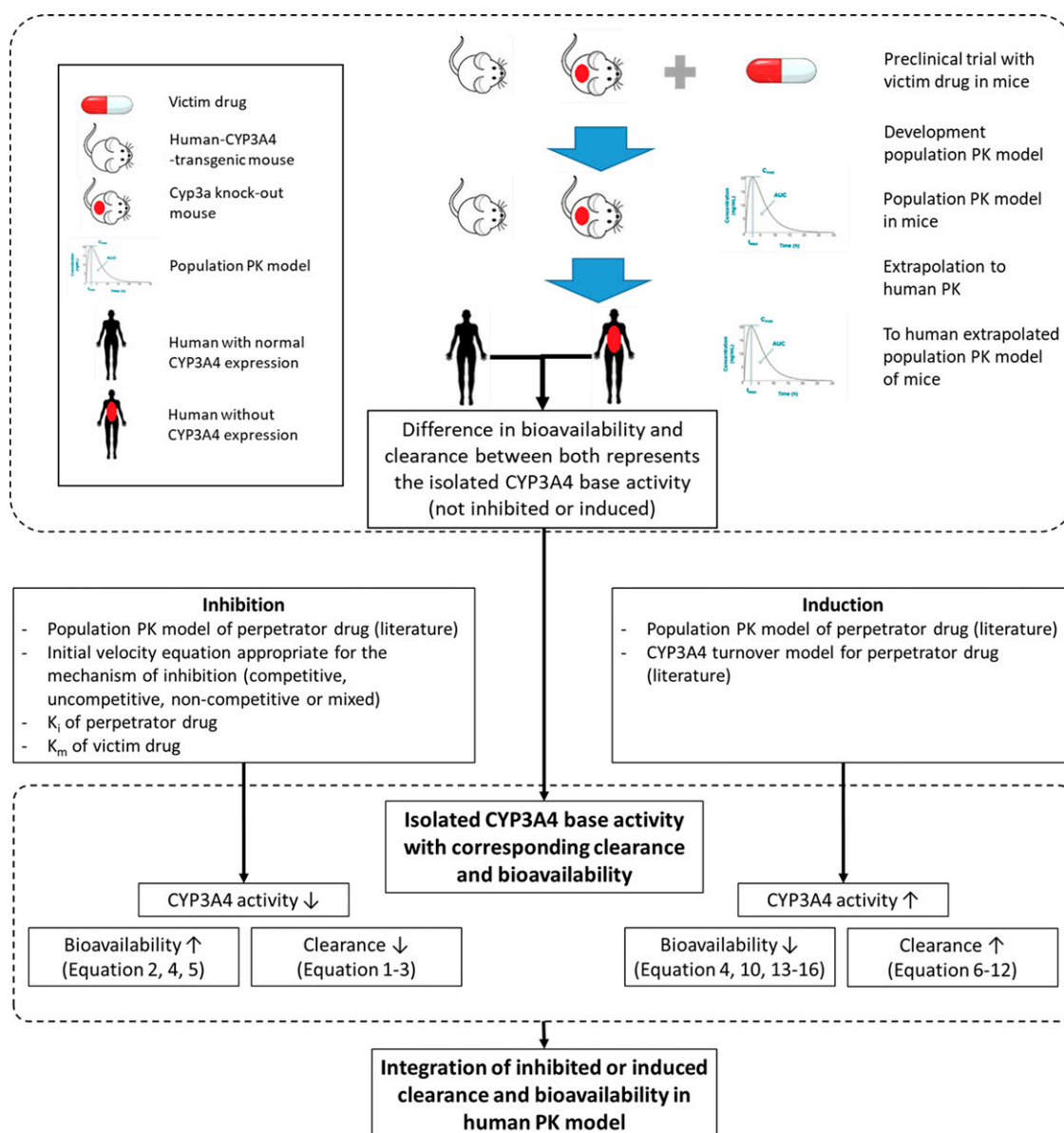
Fig. 1. Flowchart of the method for early-phase prediction of the magnitude of change in exposure for weak, moderate, and strong CYP3A4-related DDIs of small-molecule anticancer drugs. The extrapolation of mice population PK models to humans (within the dashed area) was described previously (Damoiseaux et al., 2022). K_i, dissociation constant.

First, the extraction ratio in mice (ER_{mouse}) for CYP3A4-related clearance was calculated using eq. 7. With the ER_{mouse}, $CL_{H,CYP3A4,human}$ and allometric scaling the intrinsic clearance in humans was calculated (eq. 8), assuming a mouse and human body weight (BWT) of 0.03 and 70 kg, respectively. The fraction unbound (f_u) was assumed to be similar in mouse and human. Lastly, the elimination rate constant of lorlatinib and brigatinib in the presence of an inducer could be calculated:

$$k_e = k_{e, Cyp3a\ knock-out} + \frac{CL_{H, CYP3A4, human}}{V_{human}} \quad (11)$$

where $k_{e,Cyp3a\ knockout}$ represents the elimination rate constant of the Cyp3a knockout mouse extrapolated to humans and V_{human} represents the human volume of distribution.

As for the modeling of inhibition, the difference in bioavailability between the extrapolated Cyp3a knockout and human-CYP3A4-transgenic mouse was considered the isolated CYP3A4-related metabolism of

the drug from 0% to 100%. Therefore, F_{CYP3A4} from eq. 4 applies here as well. Intestinal CYP3A4 metabolism was considered to have a significant contribution to bioavailability of brigatinib and lorlatinib. Therefore, the CYP3A4-mediated effect on bioavailability was split into two parts, metabolism due to intestinal CYP3A4 ($F_{CYP3A4,intestines}$) and the first-pass effect of liver CYP3A4. The first-pass effect of the liver was described using a one-time extraction of the $ER_{CYP3A4,human}$ from the total amount of drug that reaches the portal vein. The fraction of the bioavailability originating from intestinal CYP3A4 in a noninduced state ($F_{CYP3A4,intestines\ base}$) was calculated with ER_{mouse} (eq. 7), $F_{human-CYP3A4-transgenic}$ and $F_{Cyp3a\ knockout}$ (eq. 4):

$$F_{CYP3A4, intestines\ base} = \frac{\left(\frac{F_{human-CYP3A4-transgenic}}{F_{Cyp3a\ knock-out}}\right)}{1 - ER_{mouse}} \quad (12)$$

Although twice the amount of enzymes would be capable of metabolizing twice the amount of drug within the same time, the metabolic

TABLE 1

Clearance and bioavailability of Cyp3a knockout and human-CYP3A4-transgenic mouse for brigatinib and lorlatinib extrapolated to a 70-kg human

	Brigatinib		Lorlatinib	
	Clearance	Bioavailability	Clearance	Bioavailability
Cyp3a knockout	5.9 l/h	100%[b]	4.7 l/h	84%
Human-CYP3A4-transgenic	12.7 l/h	71%[b]	6.3 l/h	71%
CYP3A4-related clearance and bioavailability	6.8 l/h	29%[b]	1.6 l/h	13%
Human[a]	12.7 l/h (apparent oral clearance CL/F)	NA	11 l/h (single dose)	81%

[a]https://www.accessdata.fda.gov/drugsatfda_docs/nda/2017/208772Orig1s000ChemR.pdf; https://www.accessdata.fda.gov/drugsatfda_docs/nda/2018/210868Orig1s000ChemR.pdf.
[b]Relative to Cyp3a knockout mouse bioavailability.

rate in the intestines is also dependent on the drug's supply to and residence time at the enzyme site. To approximate this process without making the model unnecessarily complex, we assumed a natural logarithmic relationship between the amount of CYP3A4 enzymes in the intestines and $F_{CYP3A4,intestines}$:

$$F_{CYP3A4, intestines} = e^{\ln(F_{CYP3A4, intestines\ base}) \cdot REA} \qquad (13)$$

where the REA represents the predictions (fold change induction) of the induced CYP3A4 turnover model. The induced CYP3A4 turnover model was developed based on CYP3A4 mRNA expression and enzyme activity in human hepatocytes and therefore might not be representative for CYP3A4 induction in enterocytes (Yamashita et al., 2013). Due to the possibility that the induction in the intestines was not accurately simulated in our model, we chose to simulate both situations with and without induction of the intestines to get a better understanding of the contribution of the intestinal induction in our model.

Subsequently, the total effect of rifampicin-induced CYP3A4 on bioavailability was modeled by combining the intestinal and first-pass liver metabolized fractions from eqs. 9 and 13:

$$F = F_{CYP3A4, intestines} \cdot (1 - ER_{CYP3A4, human}) \qquad (14)$$

Simulation of DDIs. In total, 100 simulations with 10 individuals were performed for each interaction, with a randomly sampled weight corresponding to the characteristics of the clinical trial in healthy participants and without random effects (Chen et al., 2020; Patel et al., 2020; Tugnait et al., 2020). Doses and dosing schedules similar to those in clinical trials were administered in the simulation for brigatinib, lorlatinib, itraconazole, and rifampicin. Itraconazole 200 mg was administered once daily for 10 days starting 4 days (96 hours) before a single dose of lorlatinib 100 mg or brigatinib 90 mg was administered. Rifampicin 600 mg was administered once daily for 11 days starting 7 (168 hours) or 8 days (192 hours) before a single dose of brigatinib 180 mg or lorlatinib 100 mg was administered, respectively. Additionally, simulations were performed without the DDIs for brigatinib and lorlatinib in each situation.

Comparison of Predictions to Clinical Trials. The area under the plasma concentration-time curve from 0 until infinity (AUC_{0-inf}) was calculated by integration of the individually predicted concentration over time. Median AUC_{0-inf}, maximum concentration (C_{max}), and corresponding time (t_{max}) were calculated from the simulation output. Subsequently, the changes in AUC_{0-inf}, C_{max}, and t_{max} between the simulation of the DDI and monotherapy were calculated. These results were compared with clinical trial results, and the order of magnitude between both was determined. A 0.5- to 2-fold difference in the order of magnitude was considered a reasonable prediction of the DDI. To put into perspective, most predictions of competitive inhibition with PBPK models are within these margins (Kilford et al., 2022). A published framework for qualification of the Simcyp Simulator (PBPK) with respect to competitive and mechanism-based inhibition of multiple P450 enzymes evaluated

their model for CYP3A4 with 114 competitive inhibitors (Kilford et al., 2022). Comparison with clinical studies gave an average bias of 0.93 and 0.95 for C_{max} and AUC ratios, respectively. The predictions were within 1.5-fold of observed C_{max} and AUC ratios for 92% and 81%, respectively. Only four and two of the predictions were outside 2-fold of observed C_{max} and AUC ratios, respectively.

Software. Nonlinear mixed-effects modeling was performed using NONMEM (version 7.5; ICON Development Solutions, Ellicott City, MD) and Perl-speaks-NONMEM (PsN, version 5.4.0) (Beal et al., 1988). Pirana (version 2.9.9) was used as the graphical user interface for NONMEM, and R (version 4.2.1) was used for processing the data and graphical and statistical diagnostics (Keizer et al., 2013).

Results

The proportion of clearance and bioavailability attributed to CYP3A4 metabolism is presented in Table 1. In case of brigatinib, CYP3A4 was responsible for 51% of the total clearance and a 29% reduction in bioavailability, whereas CYP3A4 was responsible for a lower proportion of the total clearance and bioavailability for lorlatinib of 25% and 13%, respectively.

Concentrations over time for perpetrator drugs itraconazole and rifampicin were simulated using models from literature, and curves are presented in Supplemental Figs. 1 and 2 (Hennig et al., 2007; Wilkins et al., 2008). At steady state, the concentrations for itraconazole and rifampicin were approximately 0.2 and 2 mg/l, respectively. The CYP3A4 fold induction that resulted from the steady-state rifampicin exposure was also simulated using a model from literature and showed similar CYP3A4 induction of approximately 8-fold at steady state (Yamashita et al., 2013) (Supplemental Fig. 2).

Concentration-time curves of brigatinib and lorlatinib monotherapy and DDI predictions with itraconazole or rifampicin are shown in Fig. 2, as well as the results of clinical trials for comparison. Predictions were most accurate for the interaction with itraconazole for both brigatinib and lorlatinib (Fig. 2; Table 2). Predictions for the DDI between brigatinib and itraconazole deviated 1.07- to 1.31-fold from the results found in clinical trials for AUC_{0-inf}, C_{max}, and t_{max} based on the K_m values 0.1, 1, and 10 μM. Different K_m values within this range had minimal influence on AUC_{0-inf}, C_{max}, and t_{max}, but a K_m of 10 μM resulted in the most accurate predictions (Table 2). The predictions of the DDI between lorlatinib and itraconazole deviated only 1.11- and 0.99-fold compared with observations in clinical trials for AUC_{0-inf} and C_{max}, respectively.

Induction-related DDIs with rifampicin were less accurate, as both brigatinib and lorlatinib exposure were underpredicted and did not meet the 0.5- to 2-fold criteria (Fig. 2; Table 2). Predictions for the DDI between brigatinib and rifampicin resulted in deviations from clinical trials of 0.22-, 0.38-, and 0.83-fold for AUC_{0-inf}, C_{max}, and t_{max}, respectively (Table 2). Without intestinal induction, the predictions for the DDI between brigatinib and rifampicin resulted in deviations from clinical trials
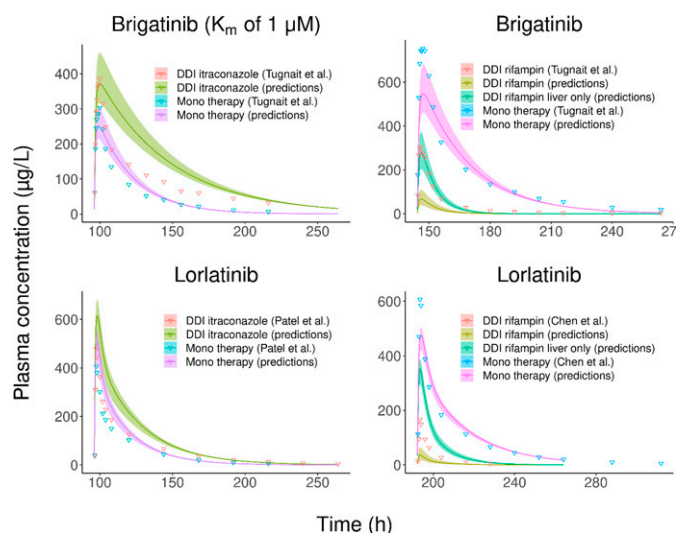
Fig. 2. Concentration-time curves of brigatinib and lorlatinib monotherapy and DDI predictions with itraconazole or rifampicin compared with results from clinical trials (Chen et al., 2020; Patel et al., 2020; Tugnait et al., 2020). For the DDI predictions involving rifampin, the senario without intestinal induction was also evaluated (referred to in the figure as liver only). A K_m of 1 μM for CYP3A4 was used for brigatinib in the prediction of the DDI with itraconazole since the actual K_m was not available.

of 0.93-, 1.27-, and 0.83-fold for AUC_{0-inf}, C_{max}, and t_{max}, respectively. For lorlatinib, the predictions of the interactions deviated 0.23- and 0.48-fold from clinical trials for AUC_{0-inf} and C_{max}, respectively. Without intestinal induction, the predictions for the DDI between lorlatinib and rifampicin resulted in deviations from clinical trials of 2.22- and 3.14-fold for AUC_{0-inf} and C_{max}, respectively.

Discussion

The magnitude of change in exposure resulting from CYP3A4 inhibition by itraconazole was adequately predicted for lorlatinib and brigatinib with an extrapolated population PK model of human-CYP3A4-transgenic mice. In contrast, the change in lorlatinib and brigatinib exposure after induction of CYP3A4 could not be accurately predicted and was underpredicted for both compounds. The reason for better prediction of inhibition is probably because inhibition of enzymes involves a limited number of variables compared with induction, making it easier to predict. Induction involves a larger set of variables, including regulation by the pregnane X receptor (PXR) and the constitutive androstane receptor (CAR) that can interact in more complex ways, potentially leading to greater unpredictability.

In our model, we used a previously published rifampicin-induced CYP3A4 turnover model that was based on CYP3A4 mRNA expression and enzyme activity in human hepatocytes (Yamashita et al., 2013). The induction of intestinal CYP3A4 was also based on this turnover model because no similar turnover model for intestinal CYP3A4 was available. Although the fundamental concept of enzyme induction is similar in both the liver and intestines, the expression of proteins involved in induction and therefore the level of induction might vary between these locations. To get a better understanding of the contribution of the intestinal induction in our model, we chose to predict both situations with induction of both liver and intestinal CYP3A4 and only liver CYP3A4. Based on the results, the induction of intestinal CYP3A4 seems to have different effects for both drugs. In case of brigatinib, predictions appear to be most accurate without the induction of intestinal CYP3A4. For lorlatinib, the results suggest that some extent of induction of intestinal CYP3A4 is required for adequate predictions. The optimal induction of intestinal CYP3A4 appears to be in between the

predictions with and without intestinal CYP3A4. Nevertheless, the predicted induction of intestinal CYP3A4 was overpredicted in our model for both drugs.

Furthermore, our assumption of a natural logarithmic relationship between the amount of CYP3A4 enzymes in the intestines and the gastrointestinal metabolism might not adequately represent the complexities of the physiological processes. This relationship has significant impact on the predictions of the bioavailability, possibly contributing to the overprediction of intestinal CYP3A4 induction. Adequate predictions of this relationship might require a more detailed model of the involved physiological processes. CYP3A4 expression levels vary throughout the intestines (Takayama et al., 2021). Brigatinib and lorlatinib are likely absorbed at different locations in the intestines because of their Biopharmaceutics Classification System classes of 1 and 4, respectively. This might clarify that both drugs undergo varying degrees of exposure to intestinal CYP3A4, leading to differences in the impact of inducing intestinal CYP3A4. Furthermore, the transit time of the drug through the intestinal wall (enterocytes) is probably important since the drug would be available to intestinal CYP3A4 for a longer period of time.

The most common way to evaluate the magnitude of change in exposure due to DDIs is through dedicated clinical trials or PBPK modeling based on clinical trial data or even after drug approval (https://www.ema.europa.eu/en/documents/scientific-guideline/guideline-investigation-drug-interactions-revision-1_en.pdf). PBPK models require substantial quantities of drug-specific data acquired from diverse in vitro and in vivo models. Subsequently, these models are further improved with clinical data and system-specific parameters. Although PBPK modeling probably results in more accurate estimates of the magnitude of change in exposure resulting from a DDI, our approach can be applied in early drug development, and, except for the required mice experiments (likely already partly available from preclinical research), the analysis is relatively easy to perform. Early detection of relevant DDIs can contribute to timely drug development decisions, prevention of unnecessary restrictions on patient enrollment, resulting in clinical study populations that are not representative of the indicated study population, and dose adjustments to ensure safety in clinical trials. Furthermore, PBPK models rely on accurate and comprehensive experimental data to make in vivo DDI predictions. The models are a simplified representation of the complex physiological processes involved in DDIs. The lack of mechanistic detail in the model carries the risk of omitting crucial physiological processes during the model development, making in vivo validation essential. In contrast, the use of extrapolated mouse models takes into account unknown physiological aspects as long as they are shared with the human physiology. Nevertheless, knocking out and humanization of mouse genes are also known to cause compensatory changes in expression of other enzymes (Kumar et al., 2017).

A limitation of this study is that it does not account for variability in CYP3A4 genotypes in the human population. The interindividual variability in CYP3A4 activity has been estimated to be attributed to genetic influences ranging from 66% to 88% (Klein and Zanger, 2013). Also, compensatory changes in Cyp3a knockout mouse models are known to upregulate other P450 enzymes such as Cyp3a13 (the only Cyp3a member not deleted) and several enzymes of the mouse Cyp2 family (Kumar et al., 2017). Consequently, Cyp3a knockout mouse models might not optimally represent a fully inhibited CYP3A4 enzyme activity for drugs that are also a substrate for one of these upregulated P450 enzymes. Furthermore, brigatinib is a known autoinductor of CYP3A4, as might be the case for other victim drugs (https://drug-interactions.medicine.iu.edu). Autoinhibition and autoinduction of target proteins such as the PXR and the CAR regulates CYP3A4 expression. These proteins differ significantly between mice and humans, which could result in misspecifications for the prediction of steady-state concentrations with and

TABLE 2

Model predictions of AUC_{0-inf}, C_{max}, and t_{max} for brigatinib and lorlatinib monotherapy and DDI with itraconazole or rifampicin compared with results from clinical trials (Chen et al., 2020; Patel et al., 2020; Tugnait et al., 2020)

Parameter		Monotherapy (Reference)	DDI (Test)	Test/Reference (%)	Difference in Fold Change (Prediction/Clinical Trial)
		Brigatinib + Itraconazole			
AUC_{0-inf} (μg/l h)	Tugnait et al., 2020	6710	14200	212	NA
	Predictions (K_m of 0.1 μM)	7230	18900	261	1.23-fold (K_m of 0.1 μM)
	Predictions (K_m of 1 μM)	7230	18500	256	1.21-fold (K_m of 1 μM)
	Predictions (K_m of 10 μM)	7230	16400	227	1.07-fold (K_m of 10 μM)
C_{max} (μg/l)	Tugnait et al., 2020	347	429	124	NA
	Predictions (K_m of 0.1 μM)	252	374	149	1.20-fold (K_m of 0.1 μM)
	Predictions (K_m of 1 μM)	252	373	148	1.19-fold (K_m of 1 μM)
	Predictions (K_m of 10 μM)	252	362	143	1.15-fold (K_m of 10 μM)
t_{max} (h)	Tugnait et al., 2020	2.8	2.6	93	NA
	Predictions (K_m of 0.1 μM)	3.2	3.9	122	1.31-fold (K_m of 0.1 μM)
	Predictions (K_m of 1 μM)	3.2	3.9	122	1.31-fold (K_m of 1 μM)
	Predictions (K_m of 10 μM)	3.2	3.7	116	1.25-fold (K_m of 10 μM)
		Brigatinib + Rifampicin			
AUC_{0-inf} (μg/l h)	Tugnait et al., 2020	16400	3140	19	NA
	Predictions	15200	645	4	0.22-fold
	Predictions (liver induction only)	15200	2690	18	0.93-fold
C_{max} (μg/l)	Tugnait et al., 2020	863	347	40	NA
	Predictions	661	102	15	0.38-fold
	Predictions (liver induction only)	661	338	51	1.27-fold
t_{max} (h)	Tugnait et al., 2020	2.5	2.0	80	NA
	Predictions	3.2	2.1	66	0.83-fold
	Predictions (liver induction only)	3.2	2.1	66	0.83-fold
		Lorlatinib + Itraconazole			
AUC_{0-inf} (μg/l h)	Patel et al., 2020	7340	10400	142	NA
	Predictions	9590	15100	158	1.11-fold
C_{max} (μg/l)	Patel et al., 2020	414	514	124	NA
	Predictions	501	614	123	0.99-fold
t_{max} (h)	Patel et al., 2020	—	—	—	NA
	Predictions	2.0	2.2	110	—
		Lorlatinib + Rifampicin			
AUC_{0-inf} (μg/l h)	Chen et al., 2020	8770	1290	15	NA
	Predictions	9170	310	3	0.23-fold
	Predictions (liver induction only)	9170	3000	33	2.22-fold
C_{max} (μg/l)	Chen et al., 2020	621	148	24	NA
	Predictions	511	59	11	0.48-fold
	Predictions (liver induction only)	511	384	75	3.14-fold
t_{max} (h)	Chen et al., 2020	—	—	—	NA
	Predictions	2.0	1.5	75	—
	Predictions (liver induction only)	2.0	1.5	75	—

—, missing data; NA, not applicable.

without DDIs (Hasegawa et al., 2011). PK information used in this study of both clinical and preclinical trials was collected after a single dose of the victim drug, and effects of autoinhibition or autoinduction are therefore unlikely. However, applications of the model in case of multiple doses should be handled with caution. Another essential point is the small number of victim and perpetrator drugs that were used in this study. It remains to be elucidated whether this approach will result in equal performance for different victim and perpetrator drugs. In relation to this, the choice of compounds that were included could be interpreted as "cherry picking," as only two of the four previously developed mouse models were selected. The misspecification in the clearance of the two not-included extrapolated mouse models was an indication that the DDI predictions with these two models were unlikely to be accurate and would not have contributed to the proof of concept. Ideally, we would have used more sensitive probes (e.g., midazolam) to evaluate our concept, but our available data were limited. Additional evaluation of this concept with such probes will be essential in future research.

An important feature of the described method is that it can also be applied to other victim drugs and, just as important, other perpetrator drugs, either weak, moderate, or strong. Extrapolation to other victim drugs will mainly be dependent on the extent to which the extrapolated human-CYP3A4-transgenic mouse is predictable for the human PK. Direct extrapolation by means of allometric scaling alone might not be sufficient for all drugs (Damoiseaux et al., 2022). However, availability of clinical PK information from phase I trials might facilitate optimization of the extrapolated mouse models to account for physiological differences that contribute to mouse and human PK differences. The extrapolation to other perpetrator drugs with an inhibitory effect on CYP3A4 can be achieved with a population PK model and an inhibitory constant of the perpetrator drug, which are often available for most well known perpetrator drugs. In the methods, we give a description of a competitive inhibition, but this method can be extended to uncompetitive, noncompetitive, or mixed inhibition by using the corresponding initial velocity equation.

To conclude, the described method offers an alternative for the early detection and assessment of potential clinical impact of CYP3A4-related DDIs. The model was able to adequately describe the inhibition of CYP3A4 metabolism and the subsequent magnitude of change in exposure. However, it was unable to accurately predict the magnitude of change in exposure of victim drugs in combination with an inducer. Additionally, the method was solely evaluated for two victim drugs and

two perpetrator drugs, leaving the performance for other victim and perpetrator drugs yet to be determined.

Data Availability

The datasets generated during and/or analyzed during the present study are available from the corresponding author on reasonable request.

Authorship Contributions

Participated in research design: Damoiseaux, Beijnen, Huitema, Dorlo.

Conducted experiments: Damoiseaux.

Performed data analysis: Damoiseaux.

Wrote or contributed to the writing of the manuscript: Damoiseaux, Beijnen, Huitema, Dorlo.

References

Beal S, Boeckmann A, and Sheiner L (1988) *NONMEM User Guides.* University of California, San Francisco, San Francisco, CA.

Chen J, Xu H, Pawlak S, James LP, Peltz G, Lee K, Ginman K, Bergeron M, and Pithavala YK (2020) The effect of rifampin on the pharmacokinetics and safety of lorlatinib: results of a phase one, open-label, crossover study in healthy participants. *Adv Ther* 37:745–758.

Damoiseaux D, Li W, Martínez-Chávez A, Beijnen JH, Schinkel AH, Huitema ADR, and Dorlo TPC (2022) Predictiveness of the human-CYP3A4-transgenic mouse model (Cyp3aXAV) for human drug exposure of CYP3A4-metabolized drugs. *Pharmaceuticals (Basel)* 15:860.

Hasegawa M, Kapelyukh Y, Tahara H, Seibler J, Rode A, Krueger S, Lee DN, Wolf CR, and Scheer N (2011) Quantitative prediction of human pregnane X receptor and cytochrome P450 3A4 mediated drug-drug interaction in a novel multiple humanized mouse line. *Mol Pharmacol* 80:518–528.

Hennig S, Waterhouse TH, Bell SC, France M, Wainwright CE, Miller H, Charles BG, and Duffull SB (2007) A d-optimal designed population pharmacokinetic study of oral itraconazole in adult cystic fibrosis patients. *Br J Clin Pharmacol* 63:438–450.

Isoherranen N, Kunze KL, Allen KE, Nelson WL, and Thummel KE (2004) Role of itraconazole metabolites in CYP3A4 inhibition. *Drug Metab Dispos* 32:1121–1131.

Keizer RJ, Karlsson MO, and Hooker A (2013) Modeling and simulation workbench for NONMEM: tutorial on Pirana, PsN, and Xpose. *CPT Pharmacometrics Syst Pharmacol* 2:e50.

Kilford PJ, Chen K-F, Crewe K, Gardner I, Hatley O, Ke AB, Neuhoff S, Zhang M, and Rowland Yeo K (2022) Prediction of CYP-mediated DDIs involving inhibition: approaches to address the requirements for system qualification of the Simcyp Simulator. *CPT Pharmacometrics Syst Pharmacol* 11:822–832.

Klein K and Zanger UM (2013) Pharmacogenomics of cytochrome P450 3A4: recent progress toward the "missing heritability" problem. *Front Genet* 4:12.

Kumar R, Mota LC, Litoff EJ, Rooney JP, Boswell WT, Courter E, Henderson CM, Hernandez JP, Corton JC, Moore DD, et al. (2017) Compensatory changes in CYP expression in three different toxicology mouse models: CAR-null, Cyp3a-null, and Cyp2b9/10/13-null mice. *PLoS One* 12:e0174355.

Lautt WW (2009) *Hepatic Circulation: Physiology and Pathophysiology,* in *Colloquium Series on Integrated Systems Physiology: From Molecule to Function to Disease* (Granger DN and Granger JP, eds) Morgan & Claypool Life Sciences, San Rafael, CA.

Molenaar-Kuijsten L, Van Balen DEM, Beijnen JH, Steeghs N, and Huitema ADR (2021) A review of CYP3A drug-drug interaction studies: practical guidelines for patients using targeted oral anticancer drugs. *Front Pharmacol* 12:670862.

Patel M, Chen J, McGrory S, O'Gorman M, Nepal S, Ginman K, and Pithavala YK (2020) The effect of itraconazole on the pharmacokinetics of lorlatinib: results of a phase I, open-label, crossover study in healthy participants. *Invest New Drugs* 38:131–139.

Takayama K, Ito K, Matsui A, Yamashita T, Kawakami K, Hirayama D, Kishimoto W, Nakase H, and Mizuguchi H (2021) In vivo gene expression profile of human intestinal epithelial cells: from the viewpoint of drug metabolism and pharmacokinetics. *Drug Metab Dispos* 49:221–232.

Tugnait M, Gupta N, Hanley MJ, Sonnichsen D, Kerstein D, Dorer DJ, Venkatakrishnan K, and Narasimhan N (2020) Effects of strong CYP2C8 or CYP3A inhibition and CYP3A induction on the pharmacokinetics of brigatinib, an oral anaplastic lymphoma kinase inhibitor, in healthy volunteers. *Clin Pharmacol Drug Dev* 9:214–223.

Wilkins JJ, Savic RM, Karlsson MO, Langdon G, McIlleron H, Pillai G, Smith PJ, and Simonsson USH (2008) Population pharmacokinetics of rifampin in pulmonary tuberculosis patients, including a semimechanistic model to describe variable absorption. *Antimicrob Agents Chemother* 52:2138–2148.

Xie C, Wei W, Zhang T, Dirsch O, and Dahmen U (2014) Monitoring of systemic and hepatic hemodynamic parameters in mice. *J Vis Exp* e51955.

Yamashita F, Sasa Y, Yoshida S, Hisaka A, Asai Y, Kitano H, Hashida M, and Suzuki H (2013) Modeling of rifampicin-induced CYP3A4 activation dynamics for the prediction of clinical drug-drug interactions from in vitro data. *PLoS One* 8:e70330.

Address correspondence to: David Damoiseaux, The Netherlands Cancer Institute, Plesmanlaan 121, 1066CX, Amsterdam, The Netherlands. E-mail: d.damoiseaux@nki.nl